Journal of Power Sources 243 (2013) 899–907

Contents lists available at SciVerse ScienceDirect

Journal of Power Sources

journal homepage: www.elsevier.com/locate/jpowsour

Stability of polymer binders in Li–O_2 batteries

Eduard Nasybulin [a], Wu Xu [a,*], Mark H. Engelhard [b], Zimin Nie [a], Xiaohong S. Li [a], Ji-Guang Zhang [a]

[a] Energy and Environment Directorate, Pacific Northwest National Laboratory, Richland, WA 99354, USA
[b] Environmental and Molecular Sciences Laboratory, Pacific Northwest National Laboratory, Richland, WA 99354, USA

HIGHLIGHTS

- Various polymer binders were investigated in Li–O_2 battery environment.
- Discharge capacity depends on binding strength and current density.
- Vinyl- and vinylidene-based polymers decompose by nucleophilic elimination.
- Carbonyl-containing polymers decompose to carbonates.
- Polyolefins and polytetrafluoroethylene are relatively stable.

GRAPHICAL ABSTRACT

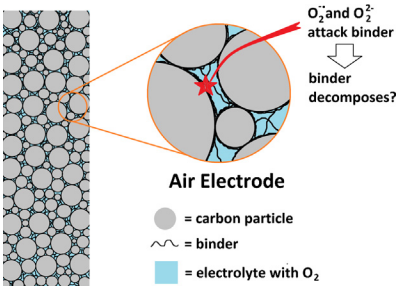

ARTICLE INFO

Article history:
Received 29 April 2013
Received in revised form
2 June 2013
Accepted 17 June 2013
Available online 24 June 2013

Keywords:
Lithium–oxygen battery
Air cathode
Binder stability
Superoxide
Peroxide

ABSTRACT

The stability of various polymer binders was systematically investigated in the oxygen-rich environment required for the operation of Li–O_2 batteries. Due to the coverage on air electrode surface by the discharge products and decomposition products of the electrolyte during the discharge process of Li–O_2 batteries, the binder in the air electrode is hard to be detected making the evaluation of its stability problematic. Therefore, stability of the binder polymers against the reduced oxygen species generated during the discharge process was investigated by ball milling the polymers with KO_2 and Li_2O_2, respectively. Most of the studied polymers are unstable under these conditions and their decomposition mechanisms are proposed according to the analyzed products. Polyethylene was found to exhibit excellent stability when exposed to superoxide and peroxide species and is suggested as a robust binder for air electrodes. In addition, the binding strength of the polymer significantly affects the discharge performance of Li–O_2 batteries.

© 2013 Elsevier B.V. All rights reserved.

1. Introduction

The theoretical gravimetric energy density of Li–O_2 batteries is 3500 Wh kg^{-1} (including mass of O_2 and considering Li_2O_2 as the only discharge product), which is much higher than the corresponding value for Li-ion batteries and is close to that of gasoline [1]. This makes Li–O_2 batteries attractive for application in electric vehicles and smart grid storage systems [2]. However, significant barriers still have to be overcome before the practical application of rechargeable Li–O_2 batteries is possible. It is well known that the reduced oxygen species ($O_2^{-\bullet}$, LiO_2, O_2^{2-}, LiO_2^-, and Li_2O_2) are generated on the cathode–electrolyte interface during the discharge process of the Li–O_2 battery [3,4]. These species are chemically reactive and may cause decomposition of all battery components, namely electrolyte (solvent, salt and additives), cathode supporting materials (substrate—typically carbon, binder and current collector), and even separator. The thickness of the layer of the insulating products generated in these side reactions grows with cycle number and leads to fast capacity fading and increase of overvoltage during the charging process.

* Corresponding author.
E-mail addresses: wu.xu@pnnl.gov (W. Xu), jiguang.zhang@pnnl.gov (J.-G. Zhang).

0378-7753/$ – see front matter © 2013 Elsevier B.V. All rights reserved.
http://dx.doi.org/10.1016/j.jpowsour.2013.06.097

In the past few years, most efforts to improve rechargeability of Li–O_2 batteries have focused on the development of stable electrolytes [5–11] while stability of the cathode has only recently attracted attention [12–14]. McCloskey et al. reported formation of Li_2CO_3 as a product of a chemical reaction between carbon and Li_2O_2 in addition to carbonates formed from the reactions between Li_2O_2 and ether-based solvents [13]. These results have been confirmed by Gallant et al. who suggested that carbon-free electrodes may improve the cycling stability [12]. Indeed, Peng et al. have achieved excellent reversibility by using a porous gold cathode substrate (without binder) in dimethyl sulfoxide-based solvent, reporting 95% capacity retention after 100 cycles [15]. However, in any practical air electrode, binder is an indispensable component contributing 10–20% to the total electrode weight. Moreover, the polymer binder is located predominantly on the surface of the conductive particles (such as carbon) rather than in the bulk. Therefore, the instability of the polymer binder may have significant effect on the performance of a Li–O_2 battery.

Polyvinylidene fluoride (PVDF) and polytetrafluoroethylene (PTFE) are the most widely used binders in air electrodes for Li–O_2 batteries reported to date. Black et al. studied the effect of chemically generated superoxide radical anions ($O_2^{-\bullet}$) on materials typically used in Li–O_2 batteries including the commonly used PVDF binder [16]. It was concluded that PVDF readily reacts with $O_2^{-\bullet}$ and undergoes dehydrofluorination with the formation of LiF and H_2O_2. H_2O_2 may further disproportionate, especially when MnO_2 is used as a catalyst, to generate H_2O and finally LiOH during discharge. Younesi et al. applied hard X-ray photoelectron spectroscopy to analyze the surface of the carbon electrode containing PVDF binder after cycling in $LiB(CN)_4$/poly(ethylene glycol) dimethyl ether electrolyte and found a significant deposit of LiF as a result of the binder decomposition [17]. LiF is a chemically and electrochemically stable compound which accumulates with cycling. Because of its insulating nature, the layer of LiF increases internal impedance of the battery, contributing to the capacity fading with cycling and increase of discharge–charge voltage hysteresis. In our recent study, we noticed that addition of Li_2O_2 to PVDF solution in *N*-methylpyrrolidone (NMP) led to quick formation of a dark-brown gel, which corresponds to the decomposition PVDF and its crosslinking [18].

The results discussed above indicate that PVDF binder is unstable during cycling of Li–O_2 batteries. PTFE is another commonly used binder for air-electrode fabrication and it is generally known as an inert polymer. However, the stability of PTFE in Li–O_2 batteries has not been studied. The stability of a polymer binder against reactive oxygen species generated during the discharge process is determined by its chemical nature. In the present work, we systematically investigated a number of polymers with various chemical structures (Fig. 1) in order to find robust binders suitable for long-term operation of Li–O_2 batteries. The stability of these polymers was studied by reacting them with potassium superoxide (KO_2) and lithium peroxide (Li_2O_2) powders, respectively, under ball milling conditions. Furthermore, the polymer binders were used in air electrodes and their effects on the discharge capacity and discharge product composition of Li–O_2 batteries were systematically investigated.

2. Experimental

2.1. Chemicals

The polymers and other chemicals used in this work were purchased from Sigma–Aldrich except as specified. The polymers included polyethylene oxide (PEO, M_w = 600,000), PTFE (DuPont), PVDF (Kyna 900, Arkema), carboxymethyl cellulose (CMC, M_w = 250,000), polyvinylpyrrolidone (PVP, M_w = 10,000), polystyrene (PS, M_w = 350,000), polyacrylonitrile (PAN, M_w = 150,000), polyvinyl chloride (PVC, M_w = 100,000), poly(-methyl methacrylate) (PMMA, M_w = 120,000), polypropylene (PP, M_w = 174,000), and polyethylene (PE, M_w = 34,000). These polymer powders were dried in a vacuum oven at 60 °C for 10 days before transferring to an MBraun glove box filled with purified argon.

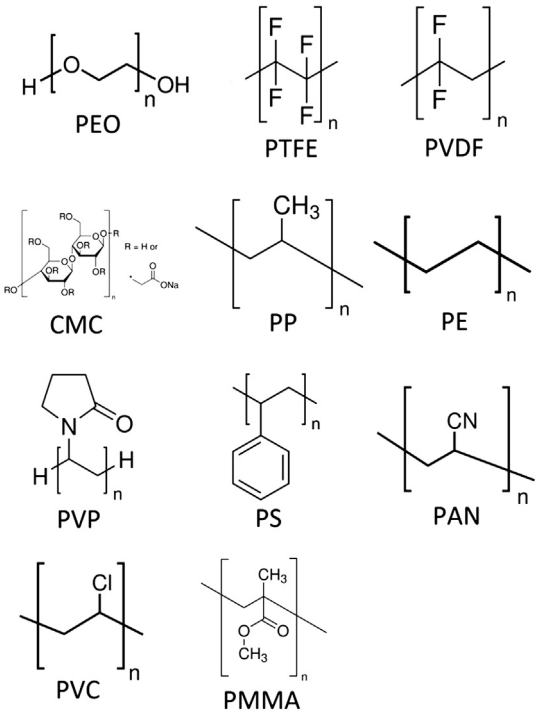

Fig. 1. Chemical structures of the used polymer binders.

KO_2, Li_2O_2 (90%), lithium chloride (LiCl), lithium fluoride (LiF, Alfa Aesar), lithium foil (99.9%, 0.75 mm thick, Alfa Aesar), acetonitrile, acetone, xylene, toluene, chloroform, dimethylformamide and tetrahydrofuran were used as received. Tetraethylene glycol dimethyl ether (tetraglyme), 1,2-dimethoxyethane (DME) and lithium bis(trifluoromethane)sulfonamide (LiTFSI) were ordered from Novolyte Technologies (all in battery grade). DME and tetraglyme were further dried over freshly activated 4 Å molecular sieves. All the chemicals were stored in the argon-filled glove box.

2.2. Stability test

Polymers were reacted with KO_2 and Li_2O_2 (oxidizers) by ball milling. In a glove box filled with purified argon, a dry polymer powder (0.40 g) was placed into the ball mill container which was made of stainless steel (SS). Either KO_2 or Li_2O_2 (0.40 g) was then added along with several SS milling balls. In addition, 0.050 g of either LiF or LiCl (for fluorine-containing polymers) was added as the internal standard for X-ray photoelectron spectroscopy (XPS) referencing. The container was closed tightly with an SS cover via a silicon O-ring and with an extra sealing cover via built-in screw threads. After that, the container was transferred out of the glove box and mounted onto a ball milling machine. Ball milling was performed for 4 h. After ball milling, the container was transferred back into the argon-filled glove box and opened inside the glove box to collect the ball-milled powder for further characterization.

2.3. Electrode preparation and battery test

Typically, 1.00 g of selected polymer was dissolved in 100 ml of the appropriate solvent with the help of heating (60 °C) in some

cases. 4.00 g Ketjenblack® (KB) carbon (Nobel Polymer Chemicals, EC-600JD) was added to the solution and mixed using a mechanical stirrer for 1 h. The as-prepared suspension was left in the open container to allow solvent evaporation; moderate heating (60 °C) was applied for the solvents with high boiling points. Details of the procedures for each of the studied polymers are listed in Table 1. The resulting composite KB/polymer (4:1) powder was sieved and used for the electrode preparation. In the case of PP, only a fraction of polymer could be dissolved in the mixture of xylenes, forming a gel-like solution, and the KB/PP ratio was 19/1 in the final composite.

A sufficient amount of KB/Polymer powder was spread on a porous Teflon® film (Interstate Specialty Products, PM6M) which served as a mechanical support and gas diffusion layer followed by cold pressing into an electrode sheet (Table 2). In some cases, a calender machine was used to prepare the air-electrode sheets. The electrodes were die-cut into disks with a diameter of 1.43 cm (and an area of 1.60 cm^2) and dried at 80 °C in a vacuum oven for 72 h. The KB carbon loading in the prepared electrodes was ~20 mg cm^{-2}.

Coin-cell type Li–O_2 batteries were assembled using perforated CR2032 SS cases (MTI Corporation) inside the glove box. A Ni mesh (Gerard Daniel Worldwide) was used as the current collector. One piece of glass fiber paper (Whatman, GF/B) and one PP membrane (Celgard, 2500) were used as separators. The electrode and separators were soaked with 240 μL of 1.0 M electrolyte of LiTFSI in tetraglyme. The assembled cells were placed in sealed Teflon containers filled with 1 atm O_2 and tested on an Arbin BT-2000 battery tester at room temperature. The discharge capacities of the batteries were measured by discharging first at a constant current of 0.05 or 0.20 mA cm^{-2} until the voltage decreased to 2.0 V and then at 2.0 V until the current density decreased to 0.02 mA cm^{-2}. The cycling stability tests of the Li–O_2 batteries were performed by running capacity-limiting (1000 mAh g^{-1}) discharge–charge cycles. The discharged batteries were disassembled in an argon-filled glove box. The discharged electrodes were removed, soaked, washed with DME three times, dried in vacuum overnight, and then analyzed by various methods.

2.4. Characterization

The surface areas of the KB/polymer powders were determined by the Brunauer–Emmett–Teller (BET) method and pore volumes were measured by Barrett–Joyner–Halenda (BJH) method, using nitrogen adsorption/desorption collected with a Quantachrome Autosorb-6B gas sorption system on degassed samples, as described in a previous report [19]. Electrochemical impedance spectroscopy (EIS) of the samples was obtained in a CHI 660D potentiostat/galvanostat. SEM images were obtained with JEOL 5900 instrument at 20 kV and secondary electron detector. X-ray diffraction (XRD) patterns of the ball-milled samples and discharged air electrodes were recorded by a D8 Advance X-ray diffractometer (Bruker AXS, Inc.). The samples were first placed in an airtight silicon crystal specimen holder (Bruker AXS, Inc.) inside the argon-filled glove box to avoid moisture contamination during sample transfer and measurement and then taken out of the glove

Table 1
Surface area, pore volume and pore size of KB carbon/binder air electrodes.

Sample	Solvent	Powder preparation	BET surface area, $m^2 g^{-1}$	BJH pore volume, cc g^{-1}	BJH pore size, Å
PEO M_w = 600,000	Acetonitrile T_b = 82 °C[a]	Cloudy solution Mixing with KB powder Solvent evaporation, 25 °C	243	1.55	20–1000
PTFE (Dupont)	Water T_b = 100 °C	Suspension Mixing with KB powder Filtering Drying, 100 °C	533.5	1.84	15–1000, peak at 20, >1000
PVDF (Kynar 900)	Acetone T_b = 56 °C	Cloudy solution Mixing with KB powder Solvent evaporation, 25 °C	489.1	2.28	15–1000, peak at 30, >1000
CMC M_w = 250,000	Water T_b = 100 °C	Clear solution Mixing with KB powder Solvent evaporation, 100 °C	545.6	1.28	10–1000, peak at 20, >1000
PP M_w = 174,000	Xylenes T_b = 140 °C	Clear gel-like solution, KB/PP = 95/5 Mixing with KB powder Solvent evaporation, 100 °C	380.4	2.24	20–1000
PE M_w = 34,000	Toluene T_b = 110.6 °C	Clear solution Mixing with KB powder Solvent evaporation, 100 °C	148.5	2.1	20–1000
PVP M_w = 10,000	Water T_b = 100 °C	Clear solution Mixing with KB powder Solvent evaporation, 100 °C	291.2	1.55	20–1000
PS M_w = 350,000	Chloroform T_b = 61.2 °C	Clear solution Mixing with KB powder Solvent evaporation, 25 °C	256.4	1.99	20–1000
PAN M_w = 150,000	DMF T_b = 153 °C	Clear solution Mixing with KB powder Precipitation with water Filtering Drying, 100 °C	301	1.85	20–1000
PVC M_w = 100,000	THF T_b = 66 °C	Clear solution Mixing with KB powder Solvent evaporation, 25 °C	223	1.87	20–1000
PMMA M_w = 120,000	Chloroform T_b = 61.2 °C	Clear solution Mixing with KB powder Solvent evaporation, 25 °C	253.6	1.81	10–1000, peak at 20, >1000

[a] T_b = boiling temperature.

Table 2
Discharge performance of Li–O_2 coin cells containing different binders.

Polymer	Electrode preparation	Discharge capacity, Ah g^{-1}		Discharge energy, Wh g^{-1}		Discharge plateau, V		Binding strength
		0.20 mA cm^{-2}	0.05 mA cm^{-2}	0.20 mA cm^{-2}	0.05 mA cm^{-2}	0.20 mA cm^{-2}	0.05 mA cm^{-2}	
PEO $M_w = 600{,}000$	2500 psi press or calender machine	1.19	2.14	2.89	5.82	2.66	2.74	Strong
PTFE (Dupont)	2500 psi press or calender machine	2.26	3.30	5.90	8.92	2.68	2.74	
PVDF (Kynar 900)	2500 psi press	2.45	2.42	6.08	6.46	2.65	2.74	
CMC $M_w = 250{,}000$	2500 psi press	0.86	0.74	2.37	1.93	2.62	2.72	
PP $M_w = 174{,}000$	2500 psi press	2.58	3.45	6.73	9.09	2.69	2.70	Medium strong
PE $M_w = 34{,}000$	2500 psi press	2.88	3.06	7.19	8.18	2.64	2.73	
PVP $M_w = 10{,}000$	2500 psi press	2.35	2.88	6.01	7.77	2.67	2.73	
PS $M_w = 350{,}000$	4000 psi press	2.01	3.59	5.03	9.64	2.63	2.72	Medium weak
PAN $M_w = 150{,}000$	4000 psi press	2.01	3.24	5.02	8.40	2.64	2.70	
PVC $M_w = 100{,}000$	4000 psi press Crush easily	2.09	2.62	5.18	6.91	2.65	2.73	Weak
PMMA $M_w = 120{,}000$	4000 psi press Crush easily	2.21	4.20	5.30	11.21	2.66	2.73	

box for the analysis. XPS measurements on the ball-milled samples and discharged electrodes were performed with a Physical Electronics Quantera scanning X-ray microprobe using the F1s peak of lithium fluoride (685.2 eV [20]) or the $Cl2p_{3/2}$ peak of lithium chloride (198.7 eV [20]) as references. The samples were transferred for XPS analyses without exposure to ambient air and the details were previously reported [9].

3. Results and discussion

3.1. Binding properties

The polymers investigated in this work cover a wide range of materials and therefore different solvents had to be used to dissolve and process them to form composite powders with KB carbon (Table 1). Solvents with polarity ranging from water ($\varepsilon = 80.1$) to toluene ($\varepsilon = 2.4$) were used depending on the chemical structure of the polymer; PTFE was the only exception since it was used in form of aqueous suspension (DuPont) because of its poor solubility in common solvents.

Surface area and pore volume of the prepared KB/polymer powders were significantly affected by the applied polymer binder (Table 1). The surface areas changed from 148.5 $m^2\ g^{-1}$ to 545.6 $m^2\ g^{-1}$ for the electrode using PE and CMC binder, respectively. The pore volume was the lowest for the electrode using CMC binder (1.28 cc g^{-1}) and the highest for the electrode using PVDF binder (2.28 cc g^{-1}). Usage of CMC, PEO and PVP binders resulted in powders with notably lower pore volumes (1.28, 1.55 and 1.55 cc g^{-1} correspondingly). SEM images of the KB/polymer powders (Fig. S1) show morphology of these electrodes on micron- and submicron-level. For the electrode prepared using PEO, PVP and especially CMC binders, smooth and dense surfaces were observed which is consistent with the lower values of the pore volume. In contrary, for the electrode prepared using PVDF, PP and PE binders, pore volumes were >2.0 cc g^{-1} and highly porous morphology was observed as shown in their SEM images (Fig. S1). The results discussed above are also consistent with EIS data (Fig. S2) as the values of interfacial resistance were the highest for the electrodes using CMC, PEO and PVP binders.

The studied polymers also showed quite different binding properties during the electrode preparation from the powders (Table 2). In the case of the binders with good binding strength, powders of the KB/polymer could be processed into free-standing electrodes by setting a pressure of 2500 psi on the manual press machine or could be rolled into sheets with the help of the calender machine. CMC possessed the strongest binding properties, apparently due to its polyelectrolytic nature. In the case of the polymers with moderate binding properties, a higher pressure of 4000 psi had to be applied. Some of the polymers (PVC and PMMA) did not work well as binders and the electrodes prepared at 4000 psi could be easily crushed under low mechanical stress. It should be noted that the observed binding strength of the studied polymers was simple qualitative evaluation. Moreover, binding strength may largely depend on molecular weight, the nature of the solvent, drying conditions, temperature of processing, etc.

3.2. Discharge performance

The discharge performance of the Li–O_2 batteries was significantly affected by the properties of the polymer binders. As shown in Table 2, the lowest discharge capacity was observed in the case of CMC (0.74 Ah g^{-1} at 0.05 mA cm^{-2}), which exhibited the strongest binding properties, and the highest discharge capacity was found in the case of PMMA (4.20 Ah g^{-1} at 0.05 mA cm^{-2}) which exhibited the weakest binding properties. In general, polymers with weaker binding properties delivered higher capacities. This phenomenon is especially evident in the case of low current density (0.05 mA cm^{-2}). This can be explained by shrinking of the porous KB structure by strong binders. Indeed, pore volume was the lowest in the case of CMC (Table 1). It should be noted that no direct correlation was found between the values of surface areas and the measured discharge capacities. This is because the surface area available for gas adsorption employed in BET method is much larger than the surface area available for wetting with electrolyte. In other words, pores below certain size may not be available for Li–O_2 reaction and are not able to hold discharge products.

Application of higher current density (0.2 mA cm^{-2}) decreased the discharge plateau by 0.05–0.1 V and resulted in a longer second discharge step at constant voltage (2.0 V), which is reflected in the calculated discharge energy values because discharge energy is a product of integrated discharge voltage and discharge capacity. The effect of binder on discharge capacity became less pronounced at higher current density because in this case the pore structures on the surface of the electrode were quickly blocked before most of the pore volume inside of the electrode could be utilized. The highest capacities were measured for PE and PP binders (2.88 and 2.58 Ah g^{-1}, respectively) which exhibit medium strength.

3.3. Discharge product analysis

The batteries with various binders were discharged at 0.20 mA cm^{-2} and disassembled for the discharge product analysis.

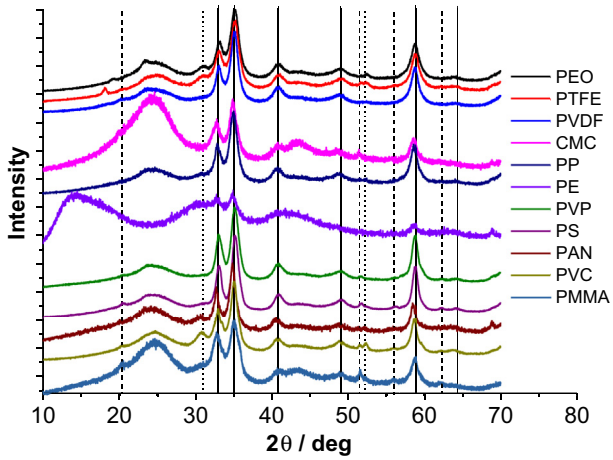

Fig. 2. XRD patterns of the discharged KB air electrodes with different binders. Solid lines represent Li_2O_2 peaks, dashed lines represent LiOH peaks, and dotted lines represent other crystalline side products.

XRD spectra of all the electrodes (Fig. 2) indicated that Li_2O_2 is the major discharge product with the characteristic peaks at $2\theta = 32.8$, 35.0, 40.8, 49.0, 58.9 and 64.2°, which is consistent with previous reports on Li–O_2 batteries when glyme-based solvents were used [5,7,9,21]. A trace amount of LiOH was identified ($2\theta = 20.4$, 51.6, 56.1, 62.3°) as a minor discharge product in the electrodes containing CMC, PMMA, PVP, PS and PVC binders. Therefore, special care should be taken in drying air electrodes, especially when hydrophilic polymers are used as binders. In addition, a pair of peaks at $2\theta = 30.9$ and 52.2° was observed corresponding to the side products. The peaks were clearly seen in the case of PVC, PEO and PTFE; however, these polymers have different chemical structures and should not lead to the same products if decomposed. It has been shown in a number of reports that tetraglyme has limited stability during discharge and decomposes to form carbonate-based and carboxylate-based side products [5,22,23]. Therefore, it is reasonable to assume that these side products come from partial decomposition of tetraglyme solvent.

XPS analysis of the discharged electrodes for several selected binders revealed Li1s and O1s peaks positioned between the binding energies of the commercial Li_2O_2 (Li1s at 54.5 and O1s at 531.1 eV) and Li_2CO_3 (Li1s at 55.1 and O1s at 531.7 eV) references (Fig. 3). Again, the positions of the peaks were only slightly affected by the selected polymer. This indicates that carbonate-based side products may contribute most to these peaks. It should be noted that XPS is a surface sensitive method and does not reflect bulk composition. It has been recently reported that Li_2O_2 may react with glyme-based solvents and form carbonates on the Li_2O_2 surface [24].

It can be concluded from the analyses of discharged electrodes that the decomposition of electrolyte plays a dominant role in the formation of side products. Together with Li_2O_2, they form deposits on the carbon electrode surface, thus masking the polymer binder and making difficult the evaluation of its stability. Moreover, the possible decomposition of binder happens on the electrode/electrolyte interface and should form only a thin (a few nm or less) layer. This makes application of bulk methods questionable due to their limited sensitivity. An alternative approach that can separate or eliminate the effect of electrolyte is desired to have more accurate determination of the binder stability against the oxygen species.

3.4. Chemical stability of binders in contact with KO_2: XRD analysis

Discharge of a Li–O_2 battery generates superoxide radical anions ($O_2^{-\bullet}$) which readily disproportionate in the presence of Li^+ to form Li_2O_2 [3]. Reactive superoxide and peroxide species ($O_2^{-\bullet}$, LiO_2, O_2^{2-}, LiO_2^-, and Li_2O_2) are responsible for the degradation of the battery components with the major contribution from the decomposition of electrolyte [5,23]. In order to evaluate the stability of binders, the effects from the decomposition of other battery components should be excluded. This was achieved by reacting polymer binders with KO_2 (as a source of $O_2^{-\bullet}$) and Li_2O_2. These reactions were difficult to perform in liquid phase because the binders investigated in this work exhibited greatly different solubility in the common solvents. Therefore solid-state reactions were carried out by ball milling.

XRD spectra of the pristine polymers and products of their ball milling with KO_2 are shown in Fig. 4a and b. It should be noted that small amounts of LiF (for non-fluorinated polymers) and LiCl (for fluorine-containing polymers) were added before ball milling for referencing the XPS spectra. Therefore, these salts as well as the products of their ion exchange with KO_2 gave corresponding peaks in the XRD spectra (Fig. 4a) confirmed with the pure reference compounds (Fig. 4c). Such peaks were not labeled in Fig. 4a; only peaks corresponding to the decomposition products were indicated.

Fig. 4a shows that PVDF (which is widely used in air-electrode preparation) is not stable in contact with $O_2^{-\bullet}$ and decomposes with the formation of KHF_2 (JCPDS #01-071-0802). Nazar and coworkers showed formation of LiF as a product of PVDF reaction with KO_2 and suggested a dehydrofluorination mechanism which was confirmed by running solid-state nuclear magnetic resonance

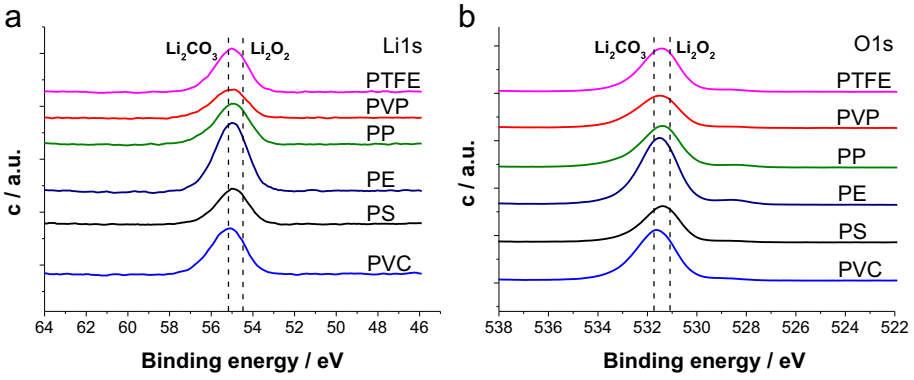

Fig. 3. XPS spectra of the discharged electrodes: (a) Li1s and (b) O1s.

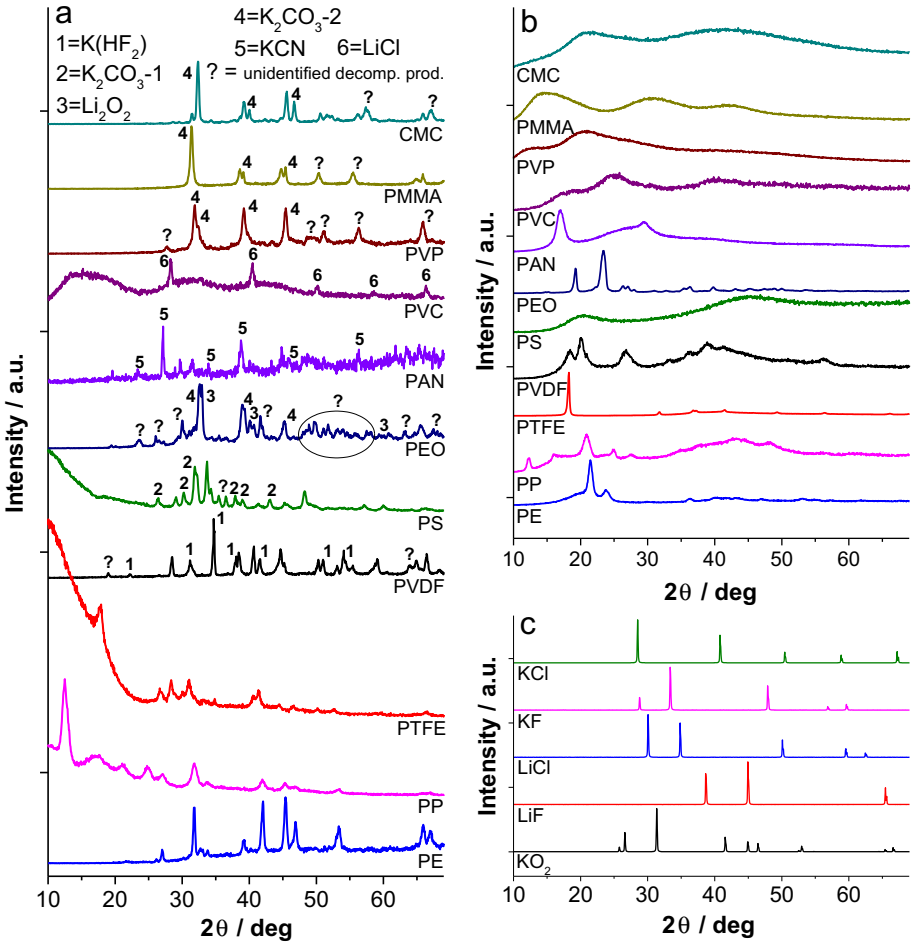

Fig. 4. XRD patterns of (a) reaction products from ball milling with KO_2, (b) pure polymers, and (c) reference compounds. Note: K_2CO_3-1 is for K_2CO_3 (JCPDS #04-014-3875) while K_2CO_3-2 is for K_2CO_3 (JCPDS #01-071-3954). The question mark "?" represents the unidentified decomposition products.

spectroscopy of the polymer residue [16]. In our work, dehydrofluorination was directly observed by the formation of KHF_2 according to the following reactions:

$$-(CH_2{-}CF_2)- \rightarrow -(CH{=}CF) + HF(\text{dehydrofluorination in the presence of } O_2{}^{-\bullet})$$

$$HF + KO_2 \rightarrow KF + HO_2$$

$$KF + HF \rightarrow KHF_2$$

$$4HO_2 \rightarrow 2H_2O + 3O_2$$

KHF_2 was obtained instead of KF because PVDF readily undergoes dehydrofluorination in the presence of strong bases [25] and was in excess to KO_2 (no KO_2 residue was detected in a ball-milled sample).

Fig. 4a also shows that PS reacted with KO_2 forming K_2CO_3 with the diffraction index of JCPDS #04-014-3875. PEO was completely unstable and decomposed to a number of products as was evidenced by the appearance of many peaks in the corresponding XRD spectrum. Among other products, Li_2O_2 and K_2CO_3 (but with another diffraction index of JCPDS #01-071-3954) could be identified. PAN was shown to undergo decyanation forming KCN while PVC was dechlorinated forming KCl. These results indicate that vinyl-based polymers are subject to nucleophilic elimination in the presence of $O_2{}^{-\bullet}$ (similarly to vinylidene-based PVDF) and therefore are not suitable for application in air electrodes. PVP, PMMA and CMC are oxygen-containing polymers with carbonyl groups and apparently underwent similar decomposition pathways eventually forming K_2CO_3 and other unidentified products which are presumably carbonate- and carboxylate-based species.

Ball milling of PVDF, PS, PEO, PAN, PVC, PVP, PMMA and CMC with KO_2 resulted in black powders and the corresponding XRD spectra demonstrated absence of KO_2, both indicating complete decomposition of these polymers. On the other hand, the other three polymers, i.e., PE, PP and PTFE, were found to be stable under the same ball milling conditions because all the peaks in their XRD spectra corresponded to KO_2 and reference compounds.

3.5. Chemical stability of binders in contact with KO_2 and Li_2O_2: XPS analysis

As discussed above, XRD investigations indicated that PVDF, PS, PEO, PAN, PVC, PVP, PMMA and CMC decompose when in contact with KO_2, while PE, PP and PTFE appear to be stable. However, XRD analysis is only sensitive to crystalline compounds and could not detect possible amorphous decomposition products. To further investigate the stability of PE, PP and PTFE, XPS was applied to analyze corresponding powders after ball milling with KO_2 and Li_2O_2. In addition to these polymers, PVDF was also tested as the

most commonly used binder. Fig. 5 shows C1s and F1s spectra of these samples. The C1s spectrum of pristine PVDF showed a pair of peaks at 290.6 (−CF_2−) and 286.2 (−CH_2−) eV of about equal intensity (Fig. 5a) which is in agreement with literature [26]. Ball milling with Li_2O_2 generated peaks at 290.1 and 284.2 eV and the latter peak also showed a shoulder at higher binding energies. Such shifts to lower binding energies indicate formation of unsaturated carbons in accordance with the dehydrofluorination mechanism. The peak at 290.1 eV was attributed to −CF═ while the peak at 284.2 eV was attributed to carbon black as a final product of dehydrofluorination with contribution from −CH═ (the shoulder). After the ball milling with KO_2, the peak at 290.6 eV disappeared and a single sharp peak at 284.2 was observed. This can be attributed to complete dehydrofluorination and formation of carbon black. The increasing intensity above 291 eV corresponded to the onset of the K2p peak of KF observed at 293.3 eV [20]. F1s spectra demonstrated a peak at 687.7 eV (−CF_2−) for the pristine PVDF (Fig. 5b). Ball milling with Li_2O_2 raised a peak at 685.6 eV mostly corresponding to LiF [20]. In the case of ball milling with KO_2, two peaks were observed, i.e., one at 683.9 eV corresponding to KF [20] and a larger one at 686.5 eV which was attributed to KHF_2.

The C1s spectrum of pristine PTFE demonstrated a −CF_2− peak at 291.8 eV [26] (Fig. 5c). Ball milling with KO_2 and Li_2O_2 resulted in appearance of additional peaks at 284.1, 285.7 and 288.1 eV (in the case of KO_2), which may indicate decomposition of PTFE. However, the −CF_2− peak at 689.0 eV observed in the F1s spectrum of pristine PTFE [26] remained nearly unchanged after ball milling (Fig. 5d). Nonetheless, there is a concern about the stability of PTFE against KO_2 and Li_2O_2.

C1s spectrum of pristine PP demonstrated a peak at 285.2 eV in agreement with literature [27] (Fig. 5e). Ball milling with Li_2O_2 and KO_2 gave small peaks at 290.0 and 289.1 eV, respectively, indicating the limited stability of PP. Appearance of these minor peaks at relatively high binding energies apparently indicates the formation of carbon–oxygen compounds. The C1s spectrum of pristine PE showed a peak at 285.0 eV in agreement with literature [28] and this peak remained unchanged after ball milling, demonstrating the excellent stability of PE against the two oxidizers (Fig. 5f).

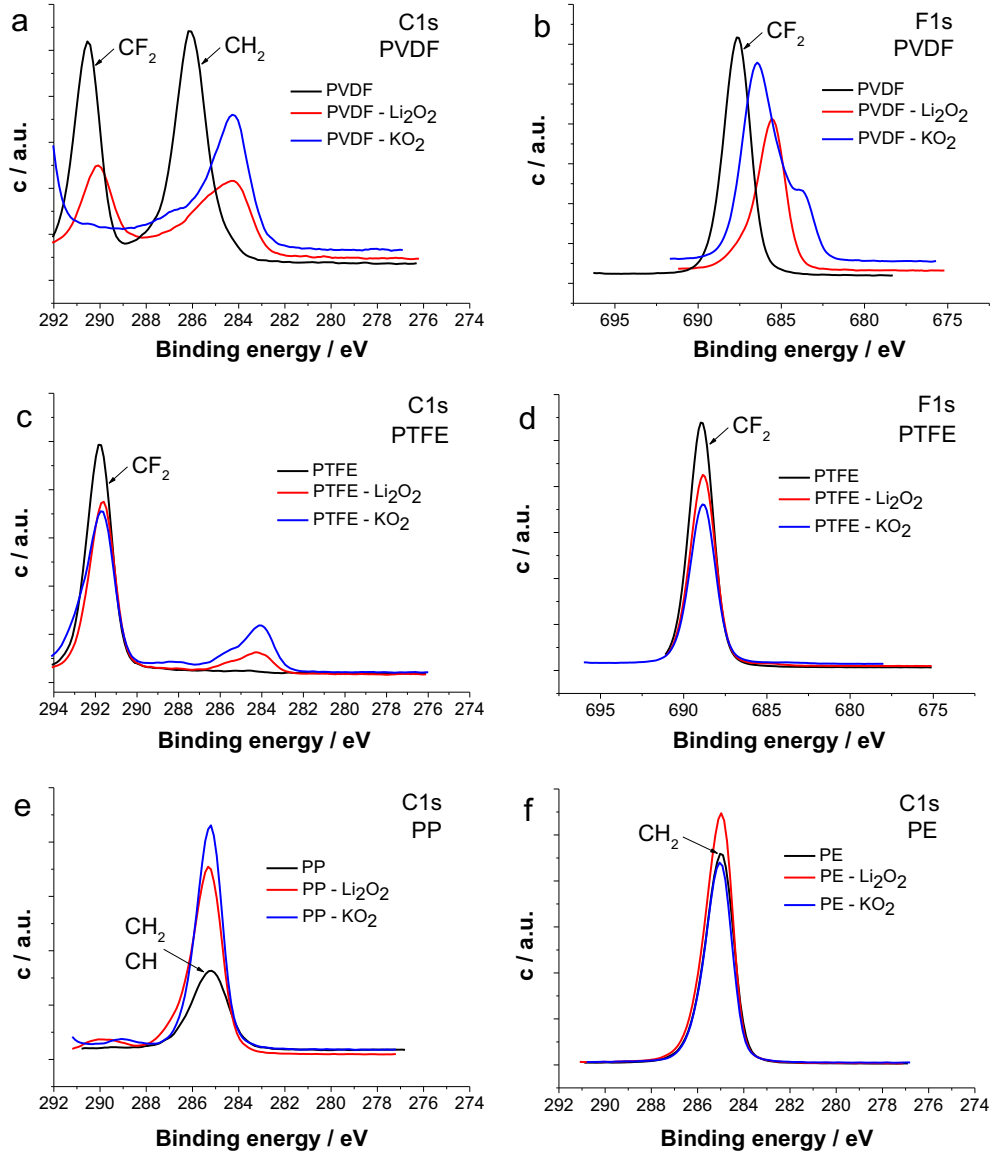

Fig. 5. XPS spectra of the reaction products and pure polymers after ball milling with KO_2 and Li_2O_2. (a) C1s for PVDF, (b) F1s for PVDF, (c) C1s for PTFE, (d) F1s for PTFE, (e) C1s for PP, and (f) C1s for PE.

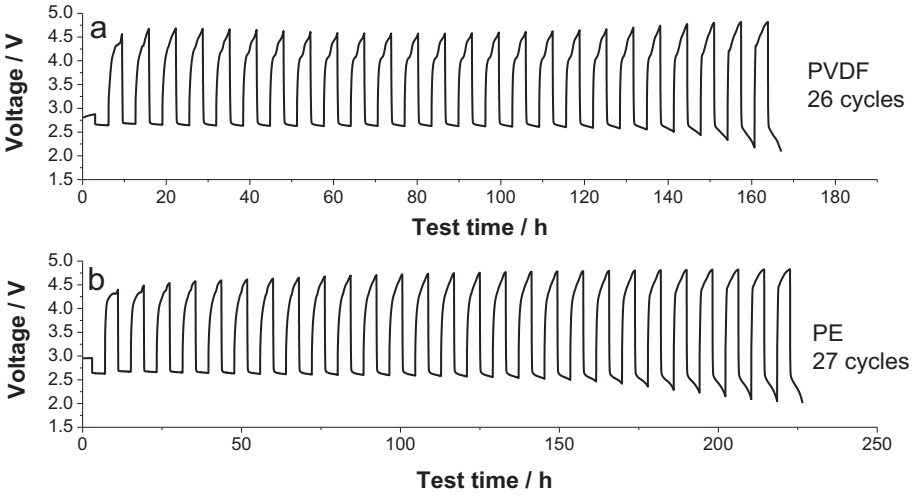

Fig. 6. 1000 mAh g^{-1} capacity-limited cycling performance of Li–O_2 batteries with (a) PVDF and (b) PE binders. Carbon loading was 1 mg cm^{-2} and current collector was carbon paper.

In summary, XPS confirmed the instability of the commonly used PVDF binder with superoxide and peroxide species. This result is consistent with the proposed dehydrofluorination mechanism. Even though PTFE, PP and PE were found to be stable by XRD analysis, XPS indicated signs of PTFE and PP decomposition when they are in contact with Li_2O_2 and KO_2. PE was found to be the only stable polymer under the applied experimental conditions. However, it should be noted that the ball milling with Li_2O_2 and KO_2 generates an environment which is more aggressive than the one encountered in a cycled Li–O_2 battery at room temperature. Therefore, some of the polymers (especially PTFE and PP) may still be suitable as binders in air-electrode preparation. Nonetheless, PE is completely stable even in the aggressive ball milling environment and therefore will certainly benefit long-term operation of Li–O_2 batteries when stable electrolytes are developed.

3.6. Effect of binder decomposition on cycling of Li–O_2 battery

PVDF and PE were selected to test how stability of the binder affects cycling performance of Li–O_2 batteries. Decomposition of binder generates side products on electrode/electrolyte interface forming insulating layer. This layer grows with cycling and may limit rechargeability of Li–O_2 batteries. In order to verify this phenomenon, KB/PVDF and KB/PE electrodes with ~1 mg cm^{-2} loading (a relatively low loading was adopted here to accelerate the cycling test) were cycled in a coin cell using LiTFSI/tetraglyme electrolyte and a capacity-limited (1 Ah g^{-1}) protocol (see Fig. 6). Although PVDF binder degrades when in contact with Li_2O_2 and KO_2, no significant difference in the cycling stability of Li–O_2 cells using the electrodes prepared with PVDF and PE binders was observed as shown in Fig. 6. One possible explanation on this apparently conflicting result is the passivation of PVDF by other side reaction products such as Li_2CO_3. Further investigations such as in situ TEM studies are required to verify this explanation.

Decompositions of the glyme-based solvents [5,9] and LiTFSI [23] have by far more pronounced effects on the degradation of electrode/electrolyte interface and fast capacity fading compared to decomposition of binder. In addition, it has been recently shown that carbon electrode is also unstable during the cycling of Li–O_2 batteries [12–14]. Nevertheless, it is obvious that there will be a demand in stable binders once stable electrolytes are developed. Here, we propose polyolefins and specifically PE as a polymer binder for air electrode preparation with exceptional stability to reduced oxygen species generated during discharge of Li–O_2 batteries. PE has an additional advantage of low T_m which makes it attractive for industrial processing of air electrodes.

4. Conclusions

Eleven polymers (PEO, PTFE, PVDF, CMC, PP, PE, PVP, PS, PAN, PVC, and PMMA) were tested as binders for carbon-based air electrodes. Binding strength depends on the nature of the polymer and significantly affects the discharge capacity. At low current densities, polymers with strong binding properties (CMC, PEO, and PVDF) decrease discharge capacity. However, the effect of the binder strength on discharge capacity is less pronounced at higher current densities. The analyses of the reaction products of Li–O_2 batteries indicates that Li_2O_2 is the major discharge product while the side products are mainly attributed to the decomposition of LiTFSI/tetraglyme electrolyte masking signs of the binder decomposition.

Stability of polymer binders against superoxide radical anions was evaluated by reacting them with KO_2 using ball milling. As evidenced by XRD analysis, PVDF, PS, PEO, PAN, PVC, PVP, PMMA and CMC decompose during ball milling with KO_2. Vinyl-based (PAN and PVC) and vinylidene-based (PVDF) polymers are subjected to nucleophilic elimination in the presence of superoxide (strong bases). Carbonyl-containing polymers (PVP, PMMA and CMC) as well as PS and PEO mainly form carbonates as a result of their decomposition.

PTFE, PP and PE were found to be stable with KO_2 by XRD analysis of the ball-milled powders. However, XPS analysis of these powders revealed signs of decomposition for PTFE and PP when in contact with KO_2 and Li_2O_2 due to the possible surface reactions and therefore their long-term stability in a strong oxidizing environment may be limited. PE was found to be the most stable polymer when exposited to superoxide and peroxide species encountered during discharge of Li–O_2 batteries. Therefore, PE is suggested as a robust binder in air electrodes suitable for long-term operation of Li–O_2 batteries.

Despite the superior chemical stability of PE against Li_2O_2 and KO_2 as compared to those of PVDF, no significant difference was observed on the cycling performance of the Li–O_2 batteries prepared using these two binders. This result can be attributed to the early passivation of the binder by the side reaction products such as Li_2CO_3 produced by the decompositions of LiTFSI/tetraglyme

electrolyte and carbon electrode during the cycling process. The decomposition of the electrolyte has much larger effects on the cycling stability of the state of the art Li–O_2 batteries. With the further development of stable electrolytes and air electrode substrates, the importance of binder stability will become more pronounced and need to be considered as one of the important design parameters for Li–O_2 batteries.

Acknowledgments

This work was supported by the Assistant Secretary for Energy Efficiency and Renewable Energy, Office of Vehicle Technology of the U.S. Department of Energy (DOE), and by the Laboratory Directed Research and Development Program at Pacific Northwest National Laboratory (PNNL), a multi-program national laboratory operated by Battelle for the U.S. DOE. The XPS measurements were performed at the Environmental Molecular Sciences Laboratory, a national scientific user facility sponsored by the DOE's Office of Biological and Environmental Research and located at PNNL.

Appendix A. Supplementary data

Supplementary data related to this article can be found at http://dx.doi.org/10.1016/j.jpowsour.2013.06.097.

References

[1] G. Girishkumar, B. McCloskey, A.C. Luntz, S. Swanson, W. Wilcke, The Journal of Physical Chemistry Letters 1 (2010) 2193–2203.
[2] M. Park, H. Sun, H. Lee, J. Lee, J. Cho, Advanced Energy Materials 2 (2012) 780–800.
[3] C.O. Laoire, S. Mukerjee, K.M. Abraham, E.J. Plichta, M.A. Hendrickson, The Journal of Physical Chemistry C 113 (2009) 20127–20134.
[4] B.D. McCloskey, R. Scheffler, A. Speidel, G. Girishkumar, A.C. Luntz, The Journal of Physical Chemistry C 116 (2012) 23897–23905.
[5] S.A. Freunberger, Y. Chen, N.E. Drewett, L.J. Hardwick, F. Barde, P.G. Bruce, Angewandte Chemie International Edition in English 50 (2011) 8609–8613.
[6] C.O. Laoire, S. Mukerjee, K.M. Abraham, E.J. Plichta, M.A. Hendrickson, The Journal of Physical Chemistry C 114 (2010) 9178–9186.
[7] B.D. McCloskey, D.S. Bethune, R.M. Shelby, G. Girishkumar, A.C. Luntz, The Journal of Physical Chemistry Letters 2 (2011) 1161–1166.
[8] B.D. McCloskey, D.S. Bethune, R.M. Shelby, T. Mori, R. Scheffler, A. Speidel, M. Sherwood, A.C. Luntz, The Journal of Physical Chemistry Letters 3 (2012) 3043–3047.
[9] W. Xu, J. Hu, M.H. Engelhard, S.A. Towne, J.S. Hardy, J. Xiao, J. Feng, M.Y. Hu, J. Zhang, F. Ding, M.E. Gross, J.-G. Zhang, Journal of Power Sources 215 (2012) 240–247.
[10] Y. Chen, S.A. Freunberger, Z. Peng, F. Barde, P.G. Bruce, Journal of the American Chemical Society 134 (2012) 7952–7957.
[11] S.A. Freunberger, Y. Chen, Z. Peng, J.M. Griffin, L.J. Hardwick, F. Barde, P. Novak, P.G. Bruce, Journal of the American Chemical Society 133 (2011) 8040–8047.
[12] B.M. Gallant, R.R. Mitchell, D.G. Kwabi, J. Zhou, L. Zuin, C.V. Thompson, Y. Shao-Horn, The Journal of Physical Chemistry C 116 (2012) 20800–20805.
[13] B.D. McCloskey, A. Speidel, R. Scheffler, D.C. Miller, V. Viswanathan, J.S. Hummelshøj, J.K. Nørskov, A.C. Luntz, The Journal of Physical Chemistry Letters 3 (2012) 997–1001.
[14] M.M. Ottakam Thotiyl, S.A. Freunberger, Z. Peng, P.G. Bruce, Journal of the American Chemical Society 135 (2013) 494–500.
[15] Z. Peng, S.A. Freunberger, Y. Chen, P.G. Bruce, Science 337 (2012) 563–566.
[16] R. Black, S.H. Oh, J.H. Lee, T. Yim, B. Adams, L.F. Nazar, Journal of the American Chemical Society 134 (2012) 2902–2905.
[17] R. Younesi, M. Hahlin, M. Treskow, J. Scheers, P. Johansson, K. Edström, The Journal of Physical Chemistry C 116 (2012) 18597–18604.
[18] W. Xu, V.V. Viswanathan, D. Wang, S.A. Towne, J. Xiao, Z. Nie, D. Hu, J.-G. Zhang, Journal of Power Sources 196 (2011) 3894–3899.
[19] W. Xu, N.L. Canfield, D. Wang, J. Xiao, Z. Nie, X.S. Li, W.D. Bennett, C.C. Bonham, J.-G. Zhang, Journal of The Electrochemical Society 157 (2010) A765.
[20] W.E. Morgan, J.R. Van Wazer, W.J. Stec, Journal of the American Chemical Society 95 (1973) 751–755.
[21] C. Laoire, S. Mukerjee, E.J. Plichta, M.A. Hendrickson, K.M. Abraham, Journal of The Electrochemical Society 158 (2011) A302–A308.
[22] M. Leskes, N.E. Drewett, L.J. Hardwick, P.G. Bruce, G.R. Goward, C.P. Grey, Angewandte Chemie International Edition in English 51 (2012) 8560–8563.
[23] E. Nasybulin, W. Xu, M.H. Engelhard, Z. Nie, S.D. Burton, L. Cosimbescu, M.E. Gross, J.-G. Zhang, The Journal of Physical Chemistry C 117 (2013) 2635–2645.
[24] R. Younesi, M. Hahlin, F. Björefors, P. Johansson, K. Edström, Chemistry of Materials 25 (2013) 77–84.
[25] H. Kise, H. Ogata, M. Nakata, Die Angewandte Makromolekulare Chemie 168 (1989) 205–216.
[26] D.T. Clark, W.J. Feast, D. Kilcast, W.K.R. Musgrave, Journal of Polymer Science: Polymer Chemistry Edition 11 (1973) 389–411.
[27] G. Barth, R. Linder, C. Bryson, Surface and Interface Analysis 11 (1988) 307–311.
[28] B.M. DeKoven, P.L. Hagans, Applied Surface Science 27 (1986) 199–213.